Experimental Thermal and Fluid Science 33 (2009) 865–874

Contents lists available at ScienceDirect

Experimental Thermal and Fluid Science

journal homepage: www.elsevier.com/locate/etfs

Looking for "laminars": Measuring intermittency on the America's Cup race course

J.R. Binns [a,*], F.O. Albina [b], I.A. Burns [b]

[a] National Centre for Maritime Engineering and Hydrodynamics, Australian Maritime College, University of Tasmania, Locked Bag 1395, Launceston, TAS 7248, Australia
[b] Design Team, BMW Oracle Racing, Muelle de la Aduana, 46024 Valencia, Spain

ARTICLE INFO

Article history:
Received 26 August 2008
Received in revised form 22 February 2009
Accepted 12 March 2009

Keywords:
Intermittency
Kurtosis
Sailing yachts
Full scale

ABSTRACT

The determination of intermittency from experimental results has been achieved in the past by a number of approximate methods, the most prolific of which involves the use of a detector function based on the square of first and second derivatives of the flow velocity with respect to time. The disadvantages of such methods are that they rely on appropriate time domain binning of the data, they are calibration dependent, they involve error propagating numerical differentiation and 50% intermittency is incorrectly diagnosed as an extremely high level of turbulence. Where experimental records are of limited time spans, calibration is difficult, measurement errors are significant and a 50% intermittency measurement is required for design purposes, the detector method loses its utility. However, recent experimental and theoretical work by Ferchichi and Tavoularis [1] has revealed a remarkably Gaussian probability distribution for the thermal passive scalar. The degree of self-similarity (analysed through the flatness of the signal) can then be used as a measure of intermittency. Flatness analysis has been used in this study on full scale data obtained experimentally on an International America's Cup Class (IACC) yacht to overcome the problems of intermittency measurement. A generalised signal conditioning technique has been proposed.

1. Introduction

The determination of intermittency levels from full scale experimental measurements is hampered by a number of very difficult problems in the maritime environment. These include

- a hostile environment which can damage instrumentation and prohibits detailed boundary layer traversing;
- the limited access points of full scale vessels, it is rare to be able to insert probes;
- the impractical nature of thermal probe calibration because of temperature variation between a controlled calibration environment and the naturally occurring experimental conditions; and
- the size and expense of full scale tests which precludes the conduct of a large number of tests.

The first problem was certainly encountered in the set of experiments detailed in the following sections. For example in the bulb experiments explained in Section 5.1, 18 out of 28 sensors failed [2]. Failure is easily characterised by either open circuit measurements or a drop to the minimum voltage value permitted by the signal conditioning unit, hence results from failed probes can be removed from further analysis. After significant investigations, it has been concluded that the only way of dealing with this problem is to use robust surface mounted probes which are cheap and easy to replace in the event of failure. Likewise the second problem is dealt with by hardware selection such that probes can be used without the need of inserting them into the structural components of full scale vessels. A solution to both of these hardware specific requirements is provided through the use of stick-on hot film probes. The use of surface hotfilm measurements for standalone transition measurement was tested by Dagenhart and Saric [3] and found to correlate with naphthalene flow visualisation and boundary layer traversing hot wire measurements. However, any potential research project is still exposed to the final two problems depending on the analysis method employed.

A common method of determining intermittency is to use a detector function of velocity measurements such as the two described in Sohn and Reshotko [4], the three described in Zhang et al. [5], the twelve listed in Bruun [6, p. 369] or a more recent one described in Franson et al. [7]. These methods compare the first and/or second differential of velocity with respect to time to certain threshold values. A summary of these methods is provided in the review of Antonia [8], in which the difficulties and subjective nature of determining threshold values are described. Time series are then examined for the amount of time spent below and above the threshold value. This method relies heavily on accurate calibration for determining the threshold exceedance value, especially when probes at different vessel locations are compared, as it is the differential with respect to time (a quantity with dimensions) that is examined for threshold exceedance. Also the method requires significant data records to obtain meaningful results, which for full scale tests can be prohibitively expensive. Finally, this

* Corresponding author. Tel.: +61 3 6335 4847; fax: +61 3 6335 4720.
E-mail address: J.Binns@amc.edu.au (J.R. Binns).

0894-1777/$ - see front matter © 2009 Elsevier Inc. All rights reserved.
doi:10.1016/j.expthermflusci.2009.03.003

method will result in an over threshold reading when 50% intermittency is recorded, reported in the data as 100% intermittency. The incorrect diagnosis of 100% intermittency results from a step change in velocity from a laminar boundary layer to a turbulent boundary layer and back again. The detector function method was found to be inadequate for use as a general interpretor of intermittency values in the full scale data obtained. Other methods of intermittency determination have used neural networks [9] and wavelet decomposition [10–12], however these too rely on accurate determination of the velocity. A method of calibration independent intermittency determination based on skewness has been developed by Struder et al. [13], however this is based completely on Tollmein–Schlichting wave propagation.

A large array of possible transition mechanisms have been proposed for a long time beginning with a review on the topic by Morkovin [14]. Within this review Morkovin explains some of the unknown input parameters which have complicated the study of transition such as three dimensional roughness and background turbulence levels. Indeed one of his main conclusions is that any design reliant on prediction of transition should incorporate a probabilistic analysis of failure to achieve laminar flow [14, p. 2]. As research on the topic has progressed, two mechanisms of transition have become accepted to describe the phenomena, being Tollmein–Schlichting wave propagation which is characterised by exponential amplification of small disturbances in otherwise highly uniform flow [15, p. 5] and bypass transition, a term first coined by Morkovin [14, p. 14] which rapidly developed into a term to describe every other form of transition. In background turbulence levels greater than 1% it has been observed experimentally and theoretically that transition occurs rapidly, effectively bypassing Tollmein–Schlichting waves [16, p. 185]. Recent work in bypass transition detailed in Durbin and Wu [17] has been able to analytically describe bypass transition giving it the more descriptive name of "continuous mode transition". The many works from this team firstly discovered that the boundary layer acts as a low-pass filter on excitation frequencies [18,19], giving a great deal of understanding to the concept of boundary layer receptivity [20,15]. However, continuous mode transition requires an interaction of disturbances of low and high frequency with an order of magnitude frequency difference [16,21]. A sailing yacht with its combined wave induced motions, structural vibration and background turbulence levels easily provides excitations with an order of magnitude difference in input frequencies [22].

The authors' have added two simple but effective steps to the analysis of flatness of a signal. The analysis of flatness as a measure of intermittency has been proposed in the past [23], but has not found the application of full scale sailing yacht experiments, for which it is ideally suited. This paper firstly examines the method of flatness as it relates to hot film measurements. Then it presents processed full scale data obtained by the authors, using hot film measurements demonstrating the generality of the method. Finally a sailing yacht keel section design example has been presented demonstrating how to use the results of these measurements. Measurement of intermittency is known to occur periodically on IACC yachts from private communications, however, publication of these studies has never occurred primarily due to the high value placed on these studies. The only known publication on the topic of full scale intermittency measurements on sailing yachts was in the work by Lurie [22].

2. The flatness measure of intermittency

A simple method of characterising an arbitrary signal according to its statistically bursty nature is to examine the signal's flatness (or kurtosis) [24, p. 124]. This underlying methodology is gaining appeal in a number of fields due to its simple and universal approach [25,26]. The same methodology can be used in determining intermittency based around the flatness of a turbulent quantity [4,24]. The conclusion that if the flow is fully turbulent then the fluctuation of turbulent quantities about their mean values will tend to a Gaussian distribution follows from Kolmogorov's 1941 hypothesis that *turbulent flow is self-similar at small scales* [24, p. 75] and was first directly proposed by Klebanoff [23]. By way of example, histograms of laminar, transitional and turbulent flow signals are shown in Fig. 3 within this paper. An examination of these plots confirms that the signals are tending to a Gaussian probability distribution function (PDF) as the flow becomes turbulent (see Section 5.1.4). Experiments in this area have been performed under controlled conditions over the past 20 years by a Canadian group, summarised by Ferchichi and Tavoularis [1]. Within this final work it is concluded that the PDF of a passive thermal scalar will tend to a Gaussian/self-similar distribution providing the heat source is kept to very low heat transfer rates. This situation exists for hot film probes, the specific PDF of hotfilm measurements is explained in Section 3.

If a signal has a Gaussian PDF, its flatness will tend to 3.0 [24, p. 125]. The flatness of a signal is the fourth moment of the distribution about the signal's mean, defined by

$$k = \sum_{i=1}^{N} \frac{(v_i - v_{\text{mean}})^4}{N(\sigma_v^2)^2} = \frac{\langle (\delta v_i^4) \rangle}{\langle (\delta v_i)^2 \rangle^2}, \tag{1}$$

where v_i is the signal at time step i, v_{mean} is the mean signal measured over N measurements and σ_v^2 is the variance of the signal for those measurements. Defined in this way the flatness is non-dimensional and independent of calibration.

As mentioned above, a fully turbulent quantity can be distinguished when the flatness tends to 3.0. In addition, an intermittent quantity (meaning a signal with only bursts of random self-similarity) can be distinguished by passing it through a high-pass filter of frequency ω. If the flatness of the signal grows without bounds as ω is increased, the signal can be said to be intermittent [24, p. 122]. Frisch [24, p. 124] also deduced that the flatness will increase with the amount of intermittency in the signal to be

$$\frac{\langle (\delta v_\gamma^4) \rangle}{\langle (\delta v_\gamma)^2 \rangle^2} = \frac{1}{\gamma} \frac{\langle (\delta v^4) \rangle}{\langle (\delta v)^2 \rangle^2}, \tag{2}$$

where δv_γ is the signal set to the mean value a fraction $1 - \gamma$ of the time. Therefore for any set of data recordings taken at various streamwise distances, applying any selected high-pass filter cut-off frequency, the flatness of each set of data will still be in order of intermittency. Gaussian and self-similar signals are not affected by raising the filter frequency [24, p. 125]. It then follows that for a signal that has been passed through a high-pass filter, the intermittency of the signal will be the flatness of the equivalent self-similar signal (3.0 for Gaussian PDF) divided by the flatness for the intermittent signal. Therefore a measure of intermittency will be (see also [23, p. 1146])

$$\gamma = \frac{3.0}{k}, \tag{3}$$

where γ is the intermittency and k is the flatness of the turbulent measurement.

2.1. The problem of flatness

Implementation of the flatness as an immediate and generic measure of intermittency runs into the problem that the signals are all sampled with inherent low-pass filtering due to probe re-

sponse and anti-aliasing filters and they are of finite time span. The finite time span aspect can be overcome as the flatness of a discrete set of data, containing N items is bounded by N [27], the proximity to N can then be used to determine the minimum intermittency measurable. Eq. (3) will then become

$$\gamma = \frac{3.0}{k} - \frac{3.0}{N}. \tag{4}$$

However, the low-pass filtering required of any data acquisition will lead to all signals being eventually registered as intermittent as the high-pass filter frequency is raised. It remains then to determine at what frequency the high-pass filter should be set. The frequency setting required for the filter is dependent on the length of the record; the longer the record the higher the maximum flatness [27].

For this study the high-pass filter was set by examining the 50% intermittency point. If it is assumed that at this point the signal will be close to a square wave sampled over a discrete number of wave periods (before filtering by the high-pass filter) then the flatness will tend to a value of 1.0 (see Appendix A and also Zhang and Yi [25, p. 902], for a demonstration). The intermittency as defined in (4) will then tend to the physically meaningless (and easily identifiable) value of 3.0. This feature has been used to identify the point along the body that is the 50% intermittency point. The signal can then be filtered with increasing frequency until an estimate of 50% intermittency is obtained at this point using (4).

3. Hotfilm measurements as a turbulent quantity

Doubt on the Gaussian nature of hotfilm measurements is certainly cast by the painstaking work of Colella and Keith [28]. Within this work Colella and Keith have accurately measured the shear stress on a surface piercing plate and concluded that it is not quite Gaussian in its distribution due to a skewness of 0.67. However, the voltage measurement of a hotfilm probe is not linearly related to the shear stress, [29,28]. When using constant temperature (CT) hot film transducers, the voltage measurement is a measure of the forced convection from interaction of the flow with the surface. The square of the voltage measurement is linearly proportional to the power required to maintain the CT surface at a constant temperature, the coefficient of linearity will be due to probe and fluid properties [29]. The linear coefficient will be the effective laminar or turbulent heat transfer coefficient which is driven by the wall normal velocity component [30]. Therefore, the square of the voltage return from the CT hot film probes will be related to the turbulent quantity of heat transfer by a linear relationship which is in turn driven by the wall normal velocity. The wall normal velocity monotonically decreases towards the wall [31] and displays a Gaussian probability distribution [32]. The novel aspect of the analysis procedure proposed here uses this unknown linear relationship to dictate possible distributions.

A probability distribution function (PDF) ($p(y)$) of one variable y is related to the PDF of x, ($f(x)$), by [33, p. 287]

$$p(y) = f(x) \times \left|\frac{\partial x}{\partial y}\right|. \tag{5}$$

If the two quantities x and y are linearly proportional then the quantity $|\partial x/\partial y|$ will be the proportional constant. Therefore, if x has a Gaussian distribution, y will also have a Gaussian distribution. As the square of the voltage measurement is linearly related to the heat transfer throughout the boundary layer it will therefore share the same distribution as the temperature throughout the boundary layer. Assuming that in a turbulent flow the square of the voltage return passed through a high-pass filter varies according to a Gaussian distribution and in a laminar flow it is constant as with the heat transfer variation, then the flatness of the square of the voltage return for N samples, will vary from 3.0 (for a turbulent flow) to 3.0/N (for a laminar flow).

4. Uncertainty in the proposed 50% intermittency location and intermittency distribution

Establishing an error estimate for the results of the analysis procedures detailed in Section 2 and the physical implementation given in Section 3 is extremely difficult given the non-linear nature of the analysis. In addition it would seem foolish to assign unnecessarily large error bounds due to linearised error estimates. Benedict and Gould [34] have provided four methods of analysing errors within turbulent quantities based on their statistical significance. The most generalised method is that of the *bootstrap* resampling method introduced by Efron in 1979. The bootstrap method has proved to provide very good agreement with analytical methods of error estimation described in Benedict and Gould [34] for simple flow statistics. This is especially the case with respect to the error estimates on higher order moments in turbulent flow measurements. Its simplicity of implementation and the high level of confidence which is obtained on the error estimate makes it the method of choice for the analysis procedures presented within this paper.

The bootstrap method proceeds by randomly replacing measurements from the original sample and recalculating the statistic of interest. The newly resampled data set is termed a *bootstrap sample* with B sets of bootstrap samples drawn from the original N measurements. B sets of the statistic of interest are therefore produced, the variation in these sets provide an estimate for the significance of the statistic given a potential variation in the original measurements. If the statistic of interest is γ then a number of new estimates for the statistic will be produced, $\gamma_{\mathrm{BOOT},i}$ where $i = 1, 2, 3, \ldots, B$. An estimate for the error (based on the statistical significance) can then be calculated by examining the variance of the bootstrap samples such that $\gamma = \bar{\gamma}_{\mathrm{BOOT}} \pm 1.96\sqrt{\sigma^2_{\gamma_{\mathrm{BOOT}}}}$ for a 95% confidence interval [34]. Errors for the intermittency values are shown in Fig. 5. Similarly, errors in the location of the 50% intermittency point have been calculated using the bootstrap method and shown in Fig. 6.

5. Results

The importance of intermittency measurements on IACC yachts is due to the "free" nature of any drag reduction obtained, resulting in faster yachts and more races won. However, there are no known publications on these studies apart from a related qualitative study performed by Lurie [22].

In the present study a set of experiments were performed on a deeply submerged body of revolution which represented a bulb. This experiment was performed to back-calculate a background turbulence level for design use. A second set of experiments were performed on an IACC keel. For all experiments a 1 kHz on-board anti-aliasing filter was used on an 8 channel CTA signal conditioning unit 54N80 as supplied by Dantec and all probes were of the single sensor type. All data acquisition was performed using a National Instruments PCMCIA mobile data acquisition system. Both sets of experiments were performed by the BMW Oracle Racing team under the direction of Dr. Binns, Dr. Albina, Mr. Burns, Mr. Frank DeBord and Mr. David LePelley (whilst in the employment of BMW Oracle Racing).

5.1. Bulb

5.1.1. Introduction

The purpose of the bulb experiment was to test the methodology for intermittency measurements on a simplified hydrodynamic

body resembling a realistic shape of interest to IACC design problems. The results of this analysis were then used to back-calculate background turbulence levels for a realistic sailing scenario.

5.1.2. Hydrodynamic platform and experimental setup

A hollow bulb (body of revolution) was fitted to the tip of a keel on a 30 ft sailing vessel. The vessel and bulb are shown in Fig. 1. A five hole pressure sensor was fitted to the nose of the bulb and calibrated analytically using vortex lattice predictions with equations presented by Gilarranz et al. [35, p. 93]. All measurements were performed on the forward half of the bulb which implies a favourable pressure gradient throughout.

5.1.3. Test setup and variables

Two sets of experiments were performed. Firstly the vessel shown in Fig. 1 was towed behind a chase boat at varied speeds to establish the viability of the method. A sample set of raw results for this set of experiments are shown in Fig. 2. Secondly a set of free sailing conditions were used to establish the effects of the variables of onset flow velocity and onset flow angle under realistic sailing conditions.

Fig. 1. The 30 ft sailing yacht used for bulb tests. The top image shows the vessel being launched. The middle image is a front view of the bulb. The lower image is a side view of the bulb, the leading edge, or nose, is on the right of the picture.

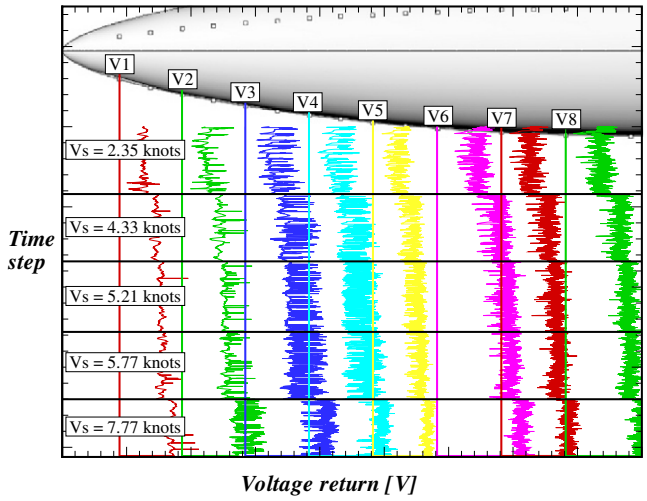

Fig. 2. Sample time trace of recorded voltages. Vertical axis is the time step of each reading (+ve down the page) for five different hull speeds as indicated. Series are offset on the horizontal axis by their position on the bulb. Bulb position is shown by the scaled graphic on top of the graph.

5.1.4. Test results

Time series results for a set of onset flow velocity variations are shown in Fig. 2. In this figure the time series run down the page. The location of the measurement points are shown as offsets to the zero reading, increasing distance from the nose of the bulb from left to right. A silhouette of the bulb shape is reproduced to scale above the graph. From this figure, and other similar runs, it is visually apparent that the heat transfer into the flow is increased with increasing speed from the gradual progression to the right of the data series with increasing velocity. It is apparent that turbulence increases with increasing velocity and with increasing distance from the nose of the bulb.

This data was used to examine the Gaussian nature of the signals from the forward probes to the aft probes. For this purpose the histograms of the data for the lowest speed are reproduced in Fig. 3. In this figure V1 is the voltage signal from the most forward probe and V8 is the most aft probe. Also plotted on these graphs are normal distribution curves for the means and variances measured. It can be seen that the signal tends towards a Gaussian signal as the probe measurements progress aft (V7 and V8). The intermittent and peaked nature of the signal can also be seen in the forward probes (V1 and V2). Finally, the double peak of medium intermittent signals can be seen in the middle probes (V3, V4, V5 and V6).

A section of the data shown in Fig. 2 is detailed in Fig. 4. From Fig. 4 it is apparent that there are two states for the signals, one at a lower heat transfer rate and a lower degree of fluctuation, the other at a higher level of heat transfer and associated fluctuation. These two states are a clear indication of a transition between a "smooth" laminar flow regime, through to a "bursty", intermittent regime and finally through to a Gaussian, random turbulent regime.

The jump between these two states creates the square wave mentioned above which corrupts potential detector function methods and decreases the flatness to a value of 1.0 at 50% intermittency. The minimum flatness can then be used to estimate the position on the body at which there is 50% intermittency. Then the signals can be passed through a high-pass filter with a cut-off frequency such that the 50% intermittency point based on the fil-

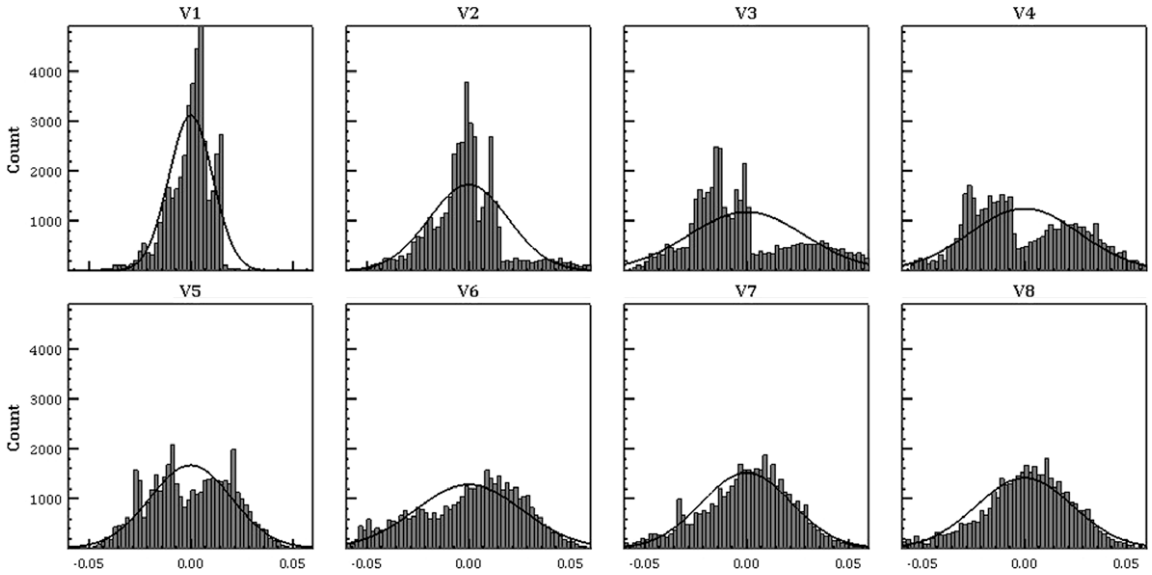

Fig. 3. Probability distribution from the first speed shown in Fig. 2. V1 is for the signal on the left of Fig. 2, V8 is for the signal on the right of Fig. 2. Line (—) shows a Gaussian PDF for the mean and variances measured for each signal. A clear trend towards two peaks at intermittent signals (V4) is apparent, with a Gaussian PDF appearing far from the nose (V8).

tered signal γ measurement of (4) coincides for a 50% intermittency. By Eq. (2), all other intermittency measurements along the bulb will then remain in order of intermittency and will provide a measure for the closeness to turbulence. This analysis has been carried out and is discussed further below.

The distribution of intermittency along the forward sections of the bulb is shown in Fig. 5 as calculated by Eq. (4) for tests in which the bulb underwent straight towing. From this data, for the Reynolds numbers tested, it can be seen that significant laminar flow is evident over regions of favourable pressure gradients.

5.1.5. Using flatness to back-calculate turbulence levels

Results for the measured 50% turbulent point along the bulb have been presented for sailing conditions in Fig. 6. The contour lines presented on this plot show analytical results for varying the background turbulence levels for the bulb with a constant pitch angle and a zero yaw angle. The analytical results were calculated using the program *3c3d* as described by Houdeville et al. [36]. The experimental data presented are for a line of probes offset from the vertical by 60°. When comparing the windward results for port tack (□) and starboard tack (■), the results show two inferred turbulence levels. The jump between two implied turbulence levels for these windward results is due to the flow on the bulb having an angle of yaw in the experiments which has not been accounted for in the predictions. However, the downwind results (△ and ▲) were measured under conditions of low yaw angle (as this is how sailing boats sail downwind), and infer a consistent background turbulence level when the starboard tack results are compared with the port tacks.

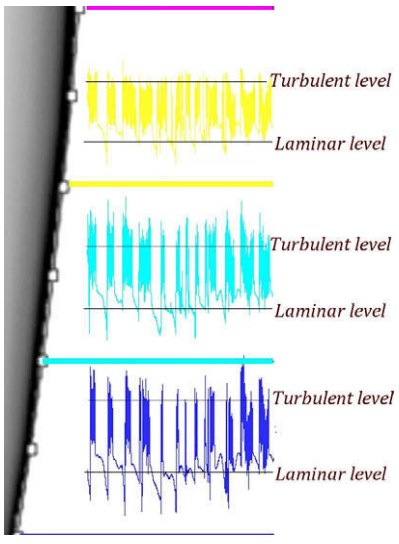

Fig. 4. Sample time trace of recorded voltages. Detail section from Fig. 2, image has been rotated such that time is increasing along the the horizontal axis. Laminar and turbulent levels of heat transfer have been marked.

5.2. Fin keel

5.2.1. Hydrodynamic platform and experimental setup

The vessel prior to docking-out is shown in Fig. 7. In the middle image of this figure the staggering of the probes can be seen, an enlarged and annotated version of this image is shown in Fig. 8. This arrangement was chosen to minimise upstream probe wake effects on the downstream probes. Due to the structural requirements of the keel (it is required to support a 19,000 kg lead bulb) it was not possible to rebate the probes. As with the bulb experiments a four hole pressure probe was installed on the leading edge of the keel and it can be seen to the left of the first hotfilm probe in Fig. 8. The four hole probe was calibrated using analytical predictions of the flow around the keel based on a vortex lattice prediction method. The measurements were performed from the nose of the foil to the start of the flap (approximately 66% of the chord). Both favourable and unfavourable pressure gradients were therefore measured.

5.2.2. Test setup and variables

The keel experiments were completed in two sets. Firstly the vessel was towed under constant keel loading and varying angle of attack by adjusting the tab angle. Secondly, measurements were taken whilst the vessel was under sail. The second set of experiments provided realistic sailing conditions to use the testing and analysis procedure.

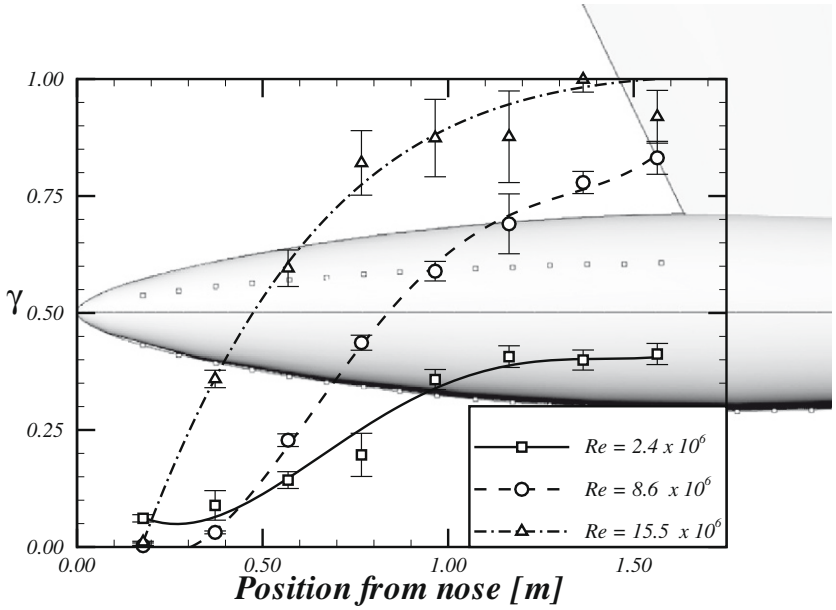

Fig. 5. Intermittency measured along the bulb for straight tow tests. The bulb silhouette behind the data has been scaled to the horizontal axis measuring from the bulb nose. At the low Reynolds number test (□), substantial laminar flow is evident right up until the keel attachment point. For the highest Reynolds number tested (Δ) the laminar flow measured is substantially diminished despite the favourable pressure gradient in the nose. Error bars have been calculated using the *bootstrap* method detailed in Section 4.

5.2.3. Test results

It is possible to construct a "universal intermittency" function for the distribution of the intermittency with respect to the non-dimensional distance along the chord of the foil. Two such functions from Narasimha and Johnson and Fashifar have been detailed in Fransson et al. [7, p. 20]. The two equations are

$$\gamma = 1 - \exp\left[-A_N(\xi + B_N)^2\right], \tag{6}$$

and

$$\gamma = 1 - \exp\left[-A_J(\xi + B_J)^3\right], \tag{7}$$

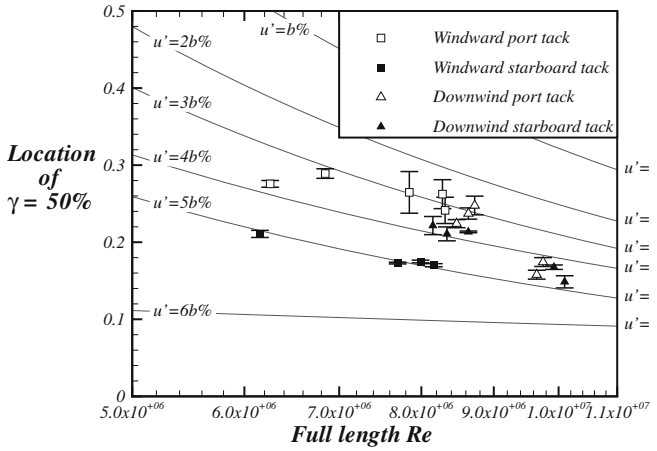

Fig. 6. Use of data to back-calculate turbulence levels for sailing conditions of windward sailing on port tack (□), starboard tack (■) and downwind on port and starboard tacks (△, ▲). Vertical axis shows location of the 50% turbulent point, increasing distance from the nose of the bulb is vertically up the page. Horizontal axis shows Reynolds number of sailing condition. Contours are predicted lines of constant turbulence instensity for zero yaw angle, where u' is the turbulence intensity from a reference velocity variation of b. Error bars have been calculated using the *bootstrap* method decribed in Section 4.

where

$$\xi = \frac{x - x_{0.5}}{x_{0.9} - x_{0.1}}. \tag{8}$$

Within these equations x_n is the chordwise location with an intermittency value of n, A_N and B_N are the coefficients of the Narasimha equation and A_J and B_J are the coefficients of the Johnson and Fashafir equation. Data for the two universal intermittency functions are presented for all of the keel measurements in Figs. 9 and 10. Fig. 9 shows the data for the downwind case for which the keel is lightly loaded. Whereas Fig. 10 shows data for the highly loaded cases in the upwind condition. Fits to the two universal equations are shown for which $A_N = 1.59$, $B_N = 0.64$, $A_J = 0.81$ and $B_J = 0.92$. These values are quite close to the values of 1.42, 0.72, 0.60 and 1.05, respectively, reported in Fransson et al. [7, p. 20]. The variation in these parameters account for the variation in turbulent spot production between the case of a flat plate in a controlled environment presented in [7] and the full scale environment used during the tests explained within this paper.

From a design perspective adherence to a universal function is important to understand the phenomena of transition, however of critical importance is the measurement of the amount of intermittency at a specified chordwise location. A sample set of test results are shown in Fig. 11 for the intermittency variation along the chord of the keel. The run presented within this graph is for a high velocity ($Re = 4.4 \times 10^6$), high keel loading sailing condition, which is common for IACC yachts. Predictions for the intermittency distribution have also been plotted using the background turbulence measurement completed during the bulb experiments. This plot demonstrates that an inferred background turbulence level from low velocity results will tend to underestimate the amount of turbulent flow at high velocity for the realistic sailing conditions measured here. Higher vessel motions at higher velocity will produce greater onset flow fluctuations, which will cause this effect.

Intermittency distributions for the pressure and suction sides of the keel are presented in Fig. 12. From this figure it can be seen that the measured intermittency distribution indicates larger regions of turbulent flow on both the suction and pressure sides of the foil. In

Fig. 7. Hydrodynamic platform for keel tests. Left image shows the vessel being launched, middle image is a side view of the keel showing the hotfilm probes. The leading edge of the keel is to the left, the four hole pressure probe fitting can be seen to the left of the first hotfilm probe. The large trim tab (flap) can be seen down the right (trailing edge) of the keel. Right image shows the vessel sailing under normal windward conditions.

addition, the degree of underestimation for the suction side is more severe than for the pressure side. The measurements indicate a very small transition region for the suction side as compared with the pressure side. The trend in under prediction of the amount of turbulence present within the strongly adverse pressure gradient of the suction side of the keel was consistent at other sailing speeds.

6. Design example

A sailing yacht is able to maintain a constant velocity through the water due to a balance between aerodynamic and hydrody-

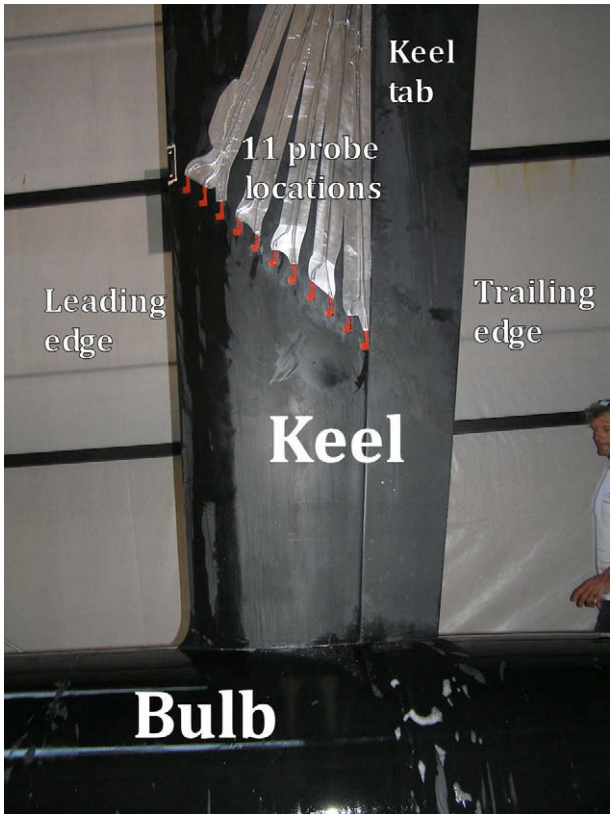

Fig. 8. Annotated detail of the keel installation (also shown in the middle image of Fig. 7).

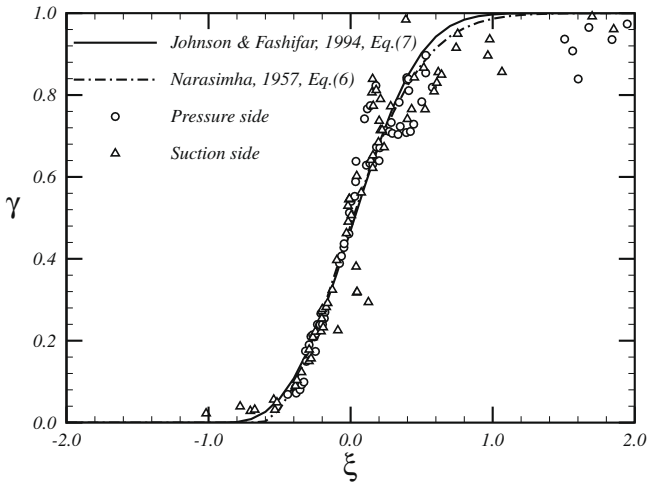

Fig. 9. Universal intermittency function for all keel measurement data sailing in the down wind condition (low lift loading). Pressure side (○) and suction side (△) of the foil shown.

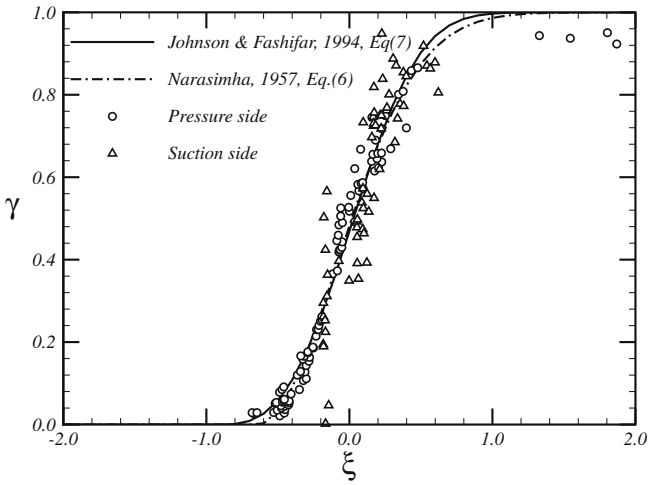

Fig. 10. Universal intermittency function for all keel measurement data sailing in the upwind condition (high lift loading). Pressure side (○) and suction side (△) of the foil shown.

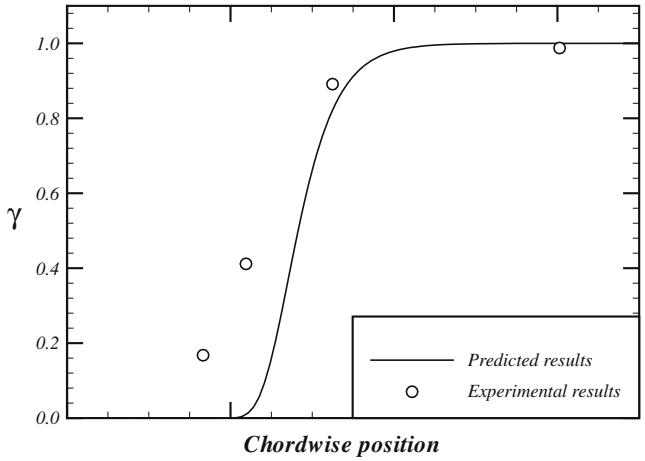

Fig. 11. Prediction and measurement of intermittency distribution along keel chord. The horizontal axis shows the position along the chord, the vertical axis shows the measured and predicted intermittency levels. Experimental results (○) and theoretical predictions (—) are shown. The predictions were performed using the background turbulence levels derived from Fig. 6. $Re = 4.4 \times 10^6$, yaw angle = −3.0°, tab angle = 12.0°.

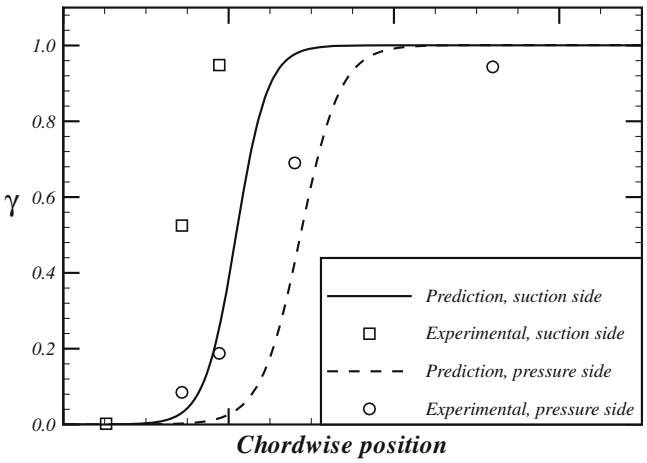

Fig. 12. Measured distribution of intermittency along the keel chord for the suction (□) and pressure side (○) measurements. Predicted intermittency distribution for suction (—) and pressure (- -) sides are also shown. The horizontal axis shows the position along the chord, the vertical axis shows the measured and predicted intermittency levels. $Re = 4.1 \times 10^6$, yaw angle = −1.0°, tab angle = 8.0°.

namic forces [37]. Initially, the sails create a side force and thrust to set the yacht in motion. As the motion increases, so too do the hydrodynamic forces created by the hull and appendages, until a balance in forces is obtained with specific lateral and longitudinal velocities. The sails, the keel and rudder act as lifting bodies in this force balance, and therefore considerable design insight can be gained by simply looking at the lift to drag ratios of these items. Although it is recognised that the optimisation of a sailing yacht is more complicated due to the non-rigid boundary conditions [38], the lift to drag ratio is certainly the best way to optimise a design detail in isolation.

To further show the application of the data and methods presented within this paper, a sample design process has been completed by the authors for an IACC keel cross section based on maximising the lift to drag ratios. The sample design answers the question of which shape from either a NACA 0018 or NACA 66-018 shape will produce the minimum amount of drag for a given amount of lift. For the purposes of this analysis the program devel-

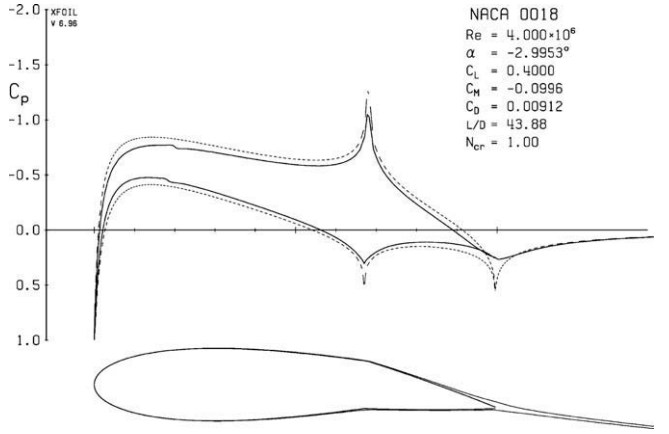

Fig. 13. NACA 0018 foil cross section, with deflected flap, used in the design example (lower figure). Upper graph shows the pressure distribution for the design case used.

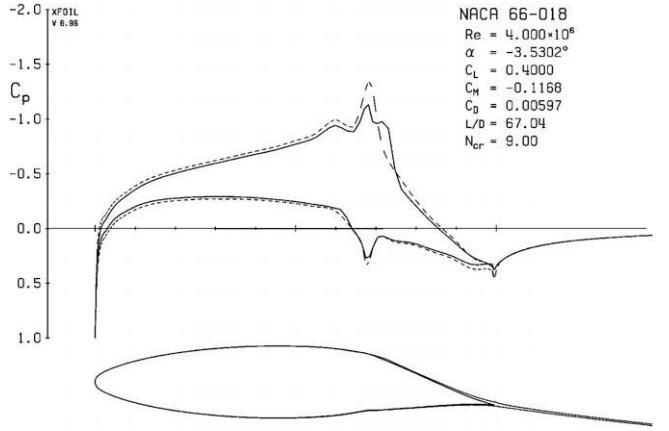

Fig. 14. NACA 66-018 foil cross section, with deflected flap, used in the design example (lower figure). Upper graph shows the pressure distribution for the design case used.

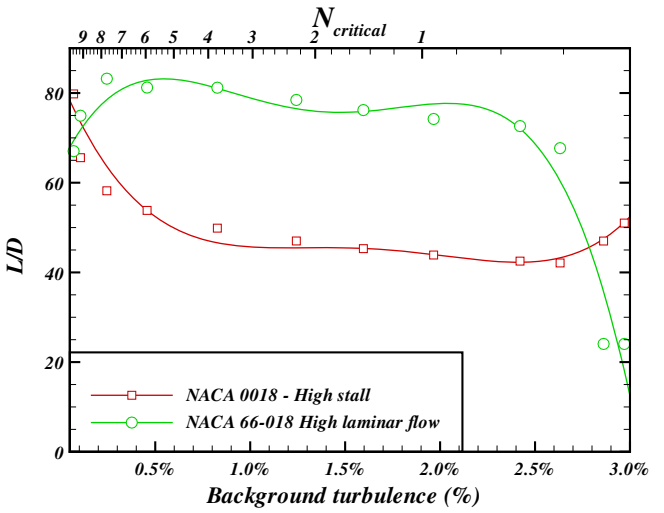

Fig. 15. Sample design use of the data measured. Vertical axis is the two dimensional lift on drag ratios for the two foil sections considered. Upper horizontal axis shows the critical amplification factor used in the analysis, lower horizontal axis shows the associated the background turbulence levels.

oped by Dr. Mark Drela called *XFoil* has been used [39,40]. Sample output from this program is presented in Figs. 13 and 14, detailing the cross sections used.

The analysis procedure assumes that a lift coefficient of 0.4 is required for the case of a 33% chord length flap deflected to 10°. The critical amplification factor used within *XFoil* was varied to simulate changes in background turbulence levels, producing a variation in lift on drag ratios. The dependence of the two dimensional lift on drag ratio on background turbulence level is plotted in Fig. 15. It should be noted that these ratios are two dimensional and would decrease significantly if three dimensional induced drag effects were incorporated into the analysis. From this figure it can be immediately concluded that at background turbulence levels below 2.5% the NACA 66-018 section produces a higher lift on drag ratio and will therefore produce a better basis for further design. If, however, the measured background turbulence level is estimated to be higher than 2.5% then the design will proceed by using a NACA 0018 section.

7. Conclusions

A method of intermittency measurement using hotfilm probes has been proposed and implemented on a full scale IACC sailing yacht. The method has been shown to be applicable to this difficult scenario and is calibration independent. Previous methods require calibrated threshold exceedance values to be determined. If calibrations vary along a test piece then variation in the threshold values are required. The method presented here effectively uses a universal and calibration independent threshold value.

Results have been used to infer background turbulence levels, which can then be used for further design of IACC appendages. The methodology has been applied to measurements on a bulb and a keel configuration demonstrating the practicality of using the self-similarity of a heat transfer signal to yield flow regime characteristics. The intermittent and self-similar nature of the measurements can be used to discriminate varying flow regimes in a consistent and robust manner.

Acknowledgements

The authors have made use of data obtained by BMW Oracle Racing SL for the 32nd America's Cup. The authors would like to thank BMW Oracle Racing for permission to use this data. A number of engineers worked on the experimental project, of particular assistance were Frank DeBord, David LePelley, Michel Kermarec, Joseph Ozanne and Alban Sabin.

Appendix A. Flatness of a square wave

For a square wave sampled over N periods, an equal amount of time will be spent an equal distance from the mean, that is $(v_i - v_{\text{mean}}) = \text{Constant}$. The variance will then be

$$\sigma^2 = \frac{1}{N}\sum (v_i - v_{\text{mean}})^2 = \frac{1}{N} N (v_i - v_{\text{mean}})^2 = (v_i - v_{\text{mean}})^2, \qquad (9)$$

therefore the square of the variance will be

$$\sigma^4 = (v_i - v_{\text{mean}})^4.$$

The flatness will then be

$$k = \sum \frac{(v_i - v_{\text{mean}})^4}{N\sigma^4} = \frac{1}{N}\sum \frac{(v_i - v_{\text{mean}})^4}{(v_i - v_{\text{mean}})^4} = \frac{1}{N} N = 1.0. \qquad (10)$$

References

[1] M. Ferchichi, S. Tavoularis, Scalar probability density function and fine structure in uniformly sheared turbulence, J. Fluid Mech. 461 (2002) 155–182.
[2] J.R. Binns, Experimental report for intermittency experiments, Technical Report, BMW Oracle Racing Internal Design Report, 2006.
[3] J.R. Dagenhart, W.S. Saric, Crossflow stability and transition experiments in swept-wing flow, Technical Report 209344, NASA Technical Publication, 1999.
[4] K.-H. Sohn, E. Reshotko, Experimental study of boundary layer transition with elevated freestream turbulence on a heated flat plate, Technical Report 187068, NASA Contractor Report, 1991.
[5] D. Zhang, Y. Chew, S. Winoto, Investigation of intermmittency measurement methods for transitional boundary layer flows, Exp. Therm. Fluid Sci. 12 (1996) 433–443.
[6] H.H. Bruun, Hot Wire Anemometry-Principles and Signal Analysis, Oxford University Press, 1995.
[7] J.H.M. Fransson, M. Matsubara, P.H. Alfredsson, Transition induced by free-stream turbulence, J. Fluid Mech. 527 (2005) 1–25.
[8] R.A. Antonia, Conditional sampling in turbulence measurement, Annu. Rev. Fluid Mech. 13 (1981) 131–156.
[9] M. Chattopadhyay, J. Dey, V. Mani, Transitional intermittency detection by neural network, Exp. Fluids 26 (1999) 549–552.
[10] M. Farge, Wavelet transforms and their applications to turbulence, Annu. Rev. Fluid Mech. 24 (1992) 395–457.
[11] J. Lewalle, D.E. Ashpis, K.-H. Sohn, Demonstration of wavelet techniques in the spectral analysis of bypass transition data, Technical Report 3555, NASA Technical Publication, 1997.
[12] C. Abid, C. Barberi-Moine, F. Papini, Application of the wavelet transform in the laminar turbulent transition for a flow in a mixed convection phenomenon, Eur. Phys. J. B 13 (2000) 707–714.
[13] G. Studer, D. Arnal, R. Houdeville, A. Seraudie, Laminar-turbulent transition in oscillating boundary layers: experimental and numerical analysis using continuous wavelet transform, Exp. Fluids 41 (2006) 685–698.
[14] M.V. Morkovin, On the many faces of transition, in: C.S. Wells (Ed.), Symposium on Viscous Drag Reduction, vol. 1, Plenum Press, 1969, pp. 1–31.
[15] L. Brandt, Numerical studies of bypass transition in the blasius boundary layer, Ph.D. thesis, Royal Institute of Technology, Stockholm, 2003.
[16] R.G. Jacobs, P.A. Durbin, Simulations of bypass transition, J. Fluid Mech. 428 (2001) 185–212.
[17] P. Durbin, X. Wu, Transition beneath vortical disturbances, Annu. Rev. Fluid Mech. 39 (2007) 107–128.
[18] R.G. Jacobs, P. Durbin, Shear sheltering and the continuous spectrum of the orr-sommerfeld equation, Phys. Fluids 10 (1998) 2006–2011.
[19] J.C.R. Hunt, P.A. Durbin, Perturbed vortical layers and shear sheltering, Fluid Dyn. Res. 24 (1999) 375–404.
[20] W.S. Saric, H.L. Reed, E.J. Kerschen, Boundary-layer receptivity to freestream disturbances, Annu. Rev. Fluid Mech. 34 (2002) 291–319.
[21] T.A. Zaki, P.A. Durbin, Mode interaction and the bypass route to transition, J. Fluid Mech. 531 (2005) 85–111.
[22] E.A. Lurie, On-the-water measurement of laminar to turbulent boundary layer transition on sailboat appendages, in: The 13th Chesapeake Sailing Yacht Symposium, vol. 13, 2001, pp. 21–26.
[23] P.S. Klebanoff, Characteristics of turbulence in a boundary layer with zero pressure gradient, Technical Report 1247, NASA Technical Report, 1954.
[24] U. Frisch, Turbulence: The Legacy of A.N. Kolmogorv, Cambridge University Press, 1995.
[25] Z.-L. Zhang, Z. Yi, Extraction of a source signal whose kurtosis value lies in a specific range, Neurocomputing 69 (2006) 900–904.
[26] R. Brychta, R. Shiavi, D. Robertson, A. Diedrich, Spike detection in human muscle sympathetic nerve activity using the kurtosis of stationary wavelet transform coefficients, J. Neurosci. Meth. 160 (2) (2007) 359–367.
[27] M. Johnson, V. Lowe, Bounds on the sample skewness and kurtosis, Technometrics 21 (3) (1979) 377–378.
[28] K. Colella, W. Keith, Measurements and scaling of wall shear stress fluctuations, Exp. Fluids 34 (2003) 253–260.
[29] B. Bellhouse, D. Schultz, Determination of mean and dynamic skin friction, separation and transition in low-speed flow with a thin-film heated element, J. Fluid Mech. 24 (1966) 379–400.
[30] P.M. Le, D.V. Papavassiliou, Turbulent dispersion from elevated sources in channel and couette flow, AIChE J. 51 (2005) 2402–2414.
[31] A. Inasawa, F. Lundell, M. Matsubara, Y. Kohama, P. Alfredsson, Velocity statistics and flow structures observed in bypass transition using stereo ptv, Exp. Fluids 34 (2003) 242–252.
[32] M. Waclawczyk, J. Pozorskia, J.-P. Minier, Probability density function computation of turbulent flows with a new near-wall model, Phys. Fluids 16 (2004) 1410–1422.
[33] W. Press, S. Teukolsky, W. Vellerling, B. Flannery, Numerical Recipes in C: The Art of Scientific Computing, Cambridge University Press, 1992.
[34] L. Benedict, R. Gould, Towards better uncertainty estimates for turbulence statistics, Exp. Fluids 22 (2) (1996) 129–136.
[35] J. Gilarranz, A. Ranz, J. Kopko, J. Sorokes, On the use of five-hole probes in the testing of industrial centrifugal compressors, J. Turbomach. 127 (2005) 91–106.

[36] R. Houdeville, P. Bardoux, V. Moreux, 3D boundary layer computations on wing-pylon-nacelle configuration, in: Workshop on Aspects of Airframe Engine Integration for Transport Aircraft, vol. 75, 1996, pp. 1–16.
[37] A. Claughton, Balance of air and water forces, in: A. Claughton, J. Wellicome, J. Shenoi (Eds.), Sailing Yacht Design-Theory, Addison Wesley Longman Ltd., Edinburgh, UK, 1998, pp. 3–13.
[38] P. Richards, T. Junge, H. Hansen, D.J.L. Pelley, F.C. Gerhardt, Optimisation of span-wise lift distributions for upwind sails, in: The 3rd High Performance Yacht Design Conference, 2008, pp. 101–110.
[39] M. Drela, M.B. Giles, Viscous-inviscid analysis of transonic and low reynolds number airfoils, AIAA J. 25 (10) (1987) 1347–1355.
[40] M. Drela, Low reynolds number aerodynamics, in: T.J. Mueller (Ed.), Lecture Notes in Engineering, vol. 54, Springer-Verlag, 1989, pp. 1–100.